

Bifurcation diagrams of axisymmetric liquid bridges of arbitrary volume in electric and gravitational axial fields

By ANTONIO RAMOS AND ANTONIO CASTELLANOS

Departamento de Electrónica y Electromagnetismo, Universidad de Sevilla,
41012 Seville, Spain

Finite-amplitude bifurcation diagrams of axisymmetric liquid bridges anchored between two plane parallel electrodes subjected to a potential difference and in the presence of an axial gravity field are found by solving simultaneously the Laplace equation for the electric potential and the Young–Laplace equation for the interface by means of the Galerkin/finite element method. Results show the strong stabilizing effect of the electric field, which plays a role somewhat similar to the inverse of the slenderness. It is also shown that the electric field may determine whether the breaking of the liquid bridge leads to two equal or unequal drops. Finally, the sensitivity of liquid bridges to an axial gravity in the presence of the electric field is studied.

1. Introduction

The statics of liquid bridges as a function of the slenderness $\lambda \equiv L/2R$ (where L is the height and R the radius) and the non-dimensional volume $\tau \equiv V/\pi R^2 L$ is well established (Martínez 1983; Sanz & Martínez 1983; Martínez 1986). The effect of gravity upon its stability is also well known (Vega & Perales 1983; Meseguer, Sanz & Perales 1990). Recently, the application of an electric field has been considered with the aim of forming longer liquid bridges. Linear bifurcation studies have shown that the electric field always increases the value of the critical liquid bridge height thus increasing the stability region (González *et al.* 1989; Ramos & Castellanos 1991). It turns out that for moderate values of electrical stresses this augmentation is approximately a linear function of the square of the applied electric field. The principal reason for the increase in liquid bridge stability is that the electric field always tends to suppress perturbations of the interface shape perpendicular to itself. This may be understood since there is a decrease in electrostatic energy stored in the system caused by these perturbations. In particular, a sinusoidal deformation of a plane interface subjected to a tangential electric field induces polarization charges that perturb the field in such a way that the total electrostatic energy decreases. An elementary estimate of this variation per unit of volume leads to $\delta W \simeq (\epsilon_1 - \epsilon_2) E \delta E < 0$ (see figure 1). Given that at equilibrium with fixed potentials the electrostatic energy has to be a maximum (Jackson 1975), the latter effect implies that dielectric forces favour an interface parallel to the electric field.

In a companion paper to this one (González & Castellanos 1993) a nonlinear bifurcation analysis is made in order to determine the way in which a cylindrical liquid bridge loses its stability in the presence of residual axial gravity. The method, based on the Lyapunov–Schmidt projection technique, is quite powerful but it is

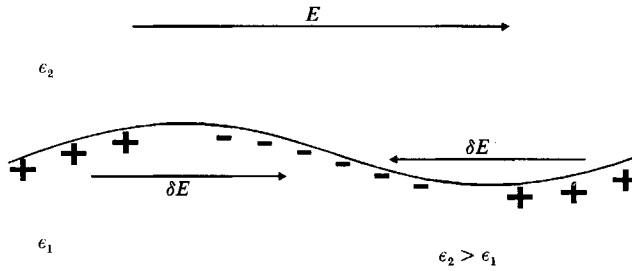


FIGURE 1. Polarization charge and electric field distributions in a sinusoidal perturbation of a planar interface subjected to a tangential field.

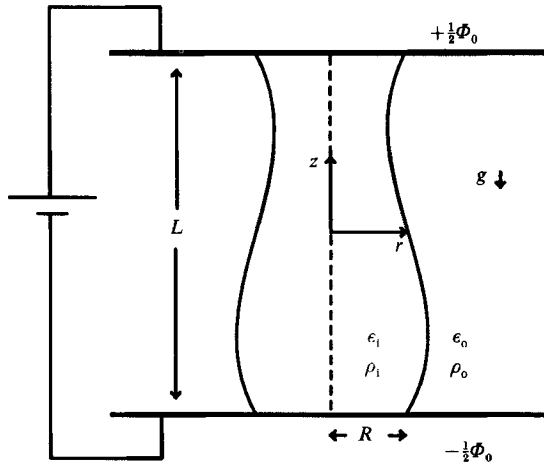


FIGURE 2. Schematic of a liquid bridge.

limited to small values of the perturbation amplitude around the cylinder and small gravitational Bond numbers.

The aim of this paper is to extend the previous work to liquid bridges of arbitrary shape and finite values of the Bond number. The problem is analytically untractable so that we have to use numerical methods to compute the finite-amplitude bifurcation diagrams. Only the minimum volume stability limit curve will be studied and, consequently, the analysis will be restricted to axisymmetric bifurcating families. Non-axisymmetric bifurcating modes of instability are important for non-rotating liquid bridges only when we are studying the maximum volume stability limit curve (Bezdeneykh, Meseguer & Perales 1992). This non-axisymmetric instability is characterized by the appearance of a bulge at the interface. For many purposes our study is sufficient in most practical situations since we are interested in elongating a given liquid bridge with the aid of electric fields keeping τ and the Bond number fixed. This physical process typically lead us to the minimum volume stability limit curve (see figures 4 and 5 in Bezdeneykh *et al.* 1992).

The bifurcation diagrams allow us to know the nonlinear stability of liquid bridges (Iooss & Joseph 1980). We have chosen a finite-element method together with first-order continuation to solve our problem. It is shown that the electric field, apart from increasing the domain of stability, may also change the symmetry of the preferred bifurcating family.

The equations and boundary conditions that govern the liquid bridge shape are presented in §2. In §3, the way that finite elements have been applied in the present problem is shown. In §4, the diagrams are drawn and conclusions about the stability obtained.

2. Formulation of the problem

Consider an insulating liquid bridge of volume V between two parallel electrodes a distance L apart and anchored on two equal disks of radius R . The anchoring is achieved by two coaxial sharp-edged rings of negligible height welded onto the electrodes so that a wide range of contact angles is allowed. This liquid bridge is surrounded by another insulating fluid and both are assumed to be immiscible. The outer medium could be the vacuum itself. The problem at hand is the determination of the equilibrium shapes and stability of the bridge when a potential difference Φ_0 is applied to the parallel electrodes and there is an axial gravity acceleration g (see figure 2).

Concerning the electric problem, since there is neither volumetric charge nor permittivity gradients in the fluids, we have to solve the Laplace equation for the electrostatic potential

$$\nabla^2\Phi = 0. \tag{1}$$

If spatial coordinates are scaled with respect to R , the electric field with respect to $E_\infty \equiv \Phi_0/L$ and the pressure with respect to σ/R ($\sigma =$ surface tension), the Young-Laplace equation augmented by the electrical pressure is written:

$$\left(\frac{1}{R_1} + \frac{1}{R_2}\right) + \chi\Delta[\frac{1}{2}\epsilon(E_t^2 - E_n^2)] + Bz + \Delta\Pi = 0. \tag{2}$$

The first term represents the capillary pressure, where R_1 and R_2 are the principal radii of curvature of the surface. The second term represents the electrostatic pressure jump, where E_t and E_n are the electric field components, tangential and normal, respectively, to the surface, ϵ is the electrical permittivity relative to the inner one, and $\chi \equiv \epsilon_1 E_\infty^2 R/\sigma$ is a non-dimensional parameter representing the ratio between electric and capillary forces. The symbol Δ stands for the jump in a quantity as we cross the interface, $\Delta X = X_o - X_i$, where subscripts refer to the outer and inner liquids. The third term takes account of the gravity force and is proportional to the Bond number defined as $gR^2(\rho_1 - \rho_o)/\sigma$ ($\rho =$ mass density). The last term represents the discontinuity of the reference pressure Π . As the media are assumed to be incompressible the electrostriction effect has not been considered.

In cylindrical coordinates, axisymmetric liquid bridge shapes are conveniently described by $r = f(z)$; where r and z are the radial and axial coordinates, respectively, and f is the shape function. The relevant boundary conditions for our configuration are:

- (i) Fixed contact lines and potentials at the electrodes:

$$f(-A) = f(A) = 1, \quad \Phi(r, -A) = -A, \quad \Phi(r, A) = A, \tag{3}$$

where Φ has been scaled with respect to $E_\infty R$.

- (ii) Axisymmetric finite potential on the axis, $r = 0$, and uniform electric field at large distance:

$$\frac{\partial\Phi}{\partial r}(0, z) = 0, \quad \lim_{r \rightarrow \infty} \frac{\partial\Phi}{\partial r}(r, z) \rightarrow 0. \tag{4}$$

(iii) Continuous potentials and normal components of the electric displacement vectors in both media across the interface:

$$\Phi_i = \Phi_o, \quad E_{ni} = \beta E_{no} \quad \text{at } r = f, \quad (5)$$

where β stands for the permittivity ratio ϵ_o/ϵ_i .

In addition, we have to include the volume constraint condition

$$\int_{-A}^A dz f^2 = 2A\tau, \quad (6)$$

noting that $\tau \equiv V/\pi R^2 L$ is the ratio between the real volume and that of the cylinder with the same R and L . Therefore, the set of unknowns is $f(z)$, $\Phi(r, z)$, $\Delta\Pi$ and the set of independent parameters is A, τ, χ, β, B .

3. Numerical analysis

The computation of liquid bridge shapes requires solving systems of equations that are nonlinear owing to the free interface, whose location is unknown. An iterative procedure is necessary to converge to a solution. Here we have used a numerical code based upon finite elements, following some ideas developed by Basaran & Scriven (1989). To use finite elements we need a bounded domain. Thus the boundary conditions at infinity have been located at a large distance, R_∞ , from the axis of symmetry.

The one-dimensional domain (liquid bridge profile) is tessellated into curve segments and the two-dimensional domain (inner and outer media) into quadrilaterals between spines $z = \text{constant}$ (Saito & Scriven 1981). Because the potential solution is not smooth at interface corners (Strang & Fix 1973), the quadrilaterals close to the contact lines have been divided into triangles. Also, the grid pitch is finer near the contact lines and increases in geometric progression with increasing distance from them (see figure 3). The introduction of these triangular elements eliminates some numerical oscillations of the electrical pressure close to the anchoring lines that appeared in a pure quadrilateral mesh. This lack of smoothness may arise because each quadrilateral attached to the contact line bears two different boundary conditions (equations (3) and (5)). The quadrilateral and triangular elements are isoparametric biquadratic of nine nodes or isoparametric quadratic of six nodes, respectively (Strang & Fix 1973). The one-dimensional elements are quadratic, exploiting the fact that they constitute the edge of the previous bidimensional elements. With these assumptions the interface and the potential are represented by

$$f(z) = \sum_{i=1}^N f_i v_i(z(\xi)), \quad (7)$$

$$\Phi(r, z) = \sum_{i=1}^M \Phi_i w_i(r(\xi, \eta), z(\xi, \eta)), \quad (8)$$

respectively, where ξ and η denote the local coordinates of the isoparametric transformation, v_i and w_i represent the one-dimensional and two-dimensional basis functions respectively and f_i and Φ_i are the values of these basis functions at the nodes.

The Galerkin weighted residuals of the augmented Young–Laplace equation and the Laplace equation are formed by weighting (2) by $f(z)v_i(z)$ and (1) by $w_i(r, z)$.

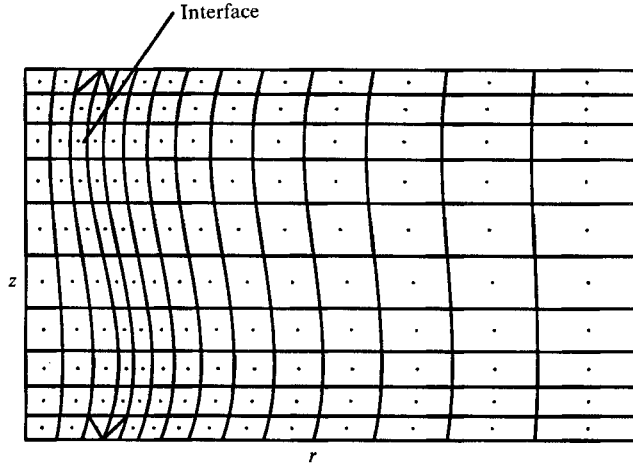


FIGURE 3. Mesh of finite elements.

Using the divergence theorem and boundary conditions to eliminate second-order derivatives we arrive at the following set of algebraic equations for f_i and Φ_i :

$$\int_{-A}^A \left((1+f_z^2)^{\frac{1}{2}} v_i + \frac{f f_z v_{z i}}{(1+f_z^2)^{\frac{1}{2}}} + (\Delta \Pi + \chi \Delta \Pi_E + Bz) f v_i \right) dz = 0 \quad (i = 1, \dots, N), \quad (9)$$

$$\int_{V_i} \nabla \Phi \cdot \nabla w_i d\tau + \beta \int_{V_0} \nabla \Phi \cdot \nabla w_i d\tau = 0 \quad (i = 1, \dots, M), \quad (10)$$

where the subscript z denotes differentiation with respect to z , Π_E stands for the electrical pressure, $\frac{1}{2}\epsilon(E_t^2 - E_n^2)$, and V_i, V_0 are the inner and outer volumes.

The Dirichlet boundary conditions (3) replace the equations associated with the nodes on the electrodes by equations of the form

$$x_i - X_i = 0, \quad (11)$$

where x_i are the unknowns f_i or Φ_i on the electrodes and X_i the known values that they take. The volume constraint forms the necessary equation to determine the unknown $\Delta \Pi$ and is given by (6). This set of algebraic equations of $N+M+1$ unknowns can be reduced to a system of $(N+1)$ unknowns by considering the electrical pressure as a function of the interfacial points, $\Pi_E = \Pi_E(f_1, \dots, f_N)$, since for a given interface the potential solution through the linear system (10) is unique.

An auxiliary equation based on the arclength parameter is included to avoid a singular Jacobian matrix when limit points appear (Keller 1977),

$$(\mathbf{x} - \mathbf{x}^*) \cdot \frac{d\mathbf{x}}{ds} \Big|_{\mathbf{x}^*} - \Delta s = 0, \quad (12)$$

and the unknowns are supplemented with λ the parameter that is being varied (either χ, τ or B). In (12), $\mathbf{x} = (f_1, \dots, f_N, \Delta \Pi, \lambda)$ is the new set of unknowns, s is the arclength of the curve described by \mathbf{x} , $d\mathbf{x}/ds$ is the unit tangent vector to the solution curve and increments are taken with respect to a previously known solution \mathbf{x}^* .

The $(N+2)$ algebraic equations are schematically written as

$$F(\mathbf{x}) = 0, \quad (13)$$

where the auxiliary equation (12) is labelled by $i = N+2$.

The derivative \mathbf{dx}/ds is obtained from the previous solution by solving

$$\mathbf{J}(\mathbf{x}^*) \cdot \mathbf{y} = \begin{bmatrix} 0 \\ \vdots \\ 0 \\ 1 \end{bmatrix}, \quad (14)$$

where $J_{ij} = \partial F_i / \partial x_j$, and $\mathbf{dx}/ds = \mathbf{y}/|\mathbf{y}|$.

The solution of the system is obtained via Newton method starting from an initial guess \mathbf{x}^0 and then calculating successive approximations in the usual way:

$$\mathbf{x}^{k+1} = \mathbf{x}^k - \mathbf{J}^{-1}(\mathbf{x}^k) \cdot \mathbf{F}(\mathbf{x}^k) \quad (k = 0, 1, 2, \dots). \quad (15)$$

The Jacobian matrix \mathbf{J} is analytically determined and is fully populated. To compute \mathbf{J} , it is necessary to evaluate the derivatives of the electrical pressure and hence the derivatives of the electric field,

$$\frac{\partial}{\partial f_j} \left(\sum_{i=1}^M \Phi_i \nabla w_i \right) = \sum_{i=1}^M \left(\frac{\partial \Phi_i}{\partial f_j} \nabla w_i + \Phi_i \frac{\partial}{\partial f_j} (\nabla w_i) \right). \quad (16)$$

If the linear system (10) is written as $\mathbf{A} \cdot \Phi = \mathbf{C}$, the derivatives $\partial \Phi_i / \partial f_j$ are computed by solving

$$\mathbf{A} \cdot \frac{\partial \Phi}{\partial f_i} = \frac{\partial \mathbf{C}}{\partial f_i} - \frac{\partial \mathbf{A}}{\partial f_i} \cdot \Phi \quad (i = 1, \dots, N), \quad (17)$$

using Cholesky factorization for the matrix \mathbf{A} (Strang & Fix 1973). The derivatives of the basis functions and the coefficients of the linear system (17) are obtained by realizing that the nodes move along the spines proportionally to the node on the interface belonging to their spine.

Since the Newton method has safe properties only if the initial guess is close to the solution a continuation method of first order has been used. We begin from a known solution, for example the cylinder, and new estimates are obtained by first-order continuation of the arclength parameter,

$$\mathbf{x}^0(s + \Delta s) = \mathbf{x}(s) + \frac{d\mathbf{x}}{ds} \Delta s. \quad (18)$$

In this way the error, defined as $\max |x_i^{k+1} - x_i^k|$, is reduced to less than 10^{-5} with two or three iterations for typical values $\Delta s = 0.01 - 0.1$. An automatic selection of Δs has been used based upon the distance from the predictor \mathbf{x}^0 to the solution \mathbf{x} .

Changes in stability are detected by the occurrence of either a shape bifurcation or a limit point (Iooss & Joseph 1980). A singularity of the Jacobian signals a bifurcation point. At a simple bifurcation, only one eigenvalue is zero. The Jacobian then passes through zero, changing its sign and so marking the location of the bifurcation. To track the new family, the critical eigenvector \mathbf{u} of the Jacobian matrix is calculated by one-step inverse iteration and the initial estimate for the new branch is the critical solution plus a small vector in the direction of the eigenvector (Basaran & Scriven 1989),

$$\mathbf{x}^0(s^* + \Delta s) = \mathbf{x}(s^*) + \mathbf{u} \Delta s, \quad (19)$$

and equation (12) is substituted by

$$(\mathbf{x} - \mathbf{x}^*) \cdot \mathbf{u} - \Delta s = 0. \quad (20)$$

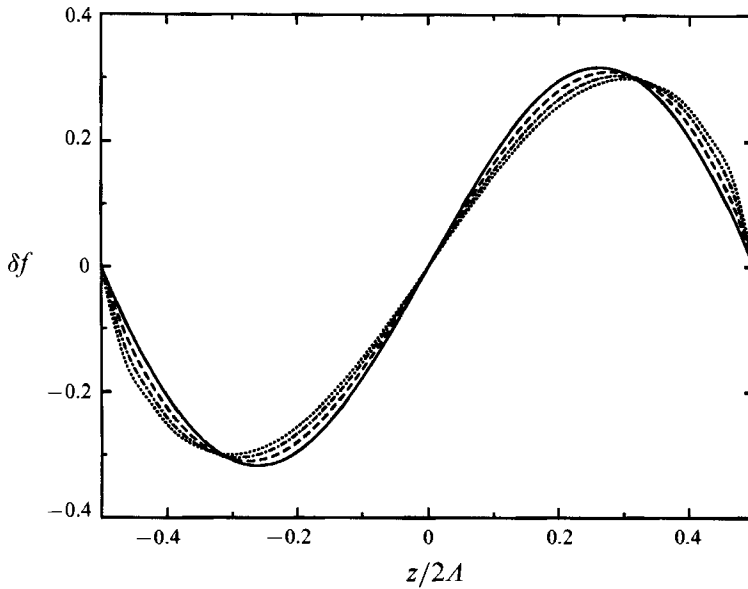


FIGURE 4. Critical eigenvector shapes for different A : —, $A = 4$; ---, $A = 5$; - · -, $A = 6$; ···, $A = 7$.

Slenderness A	Bifurcation electrical number χ_a (analytical)	Bifurcation electrical number χ_{FE} (finite element)	% relative error $100 (\chi_a - \chi_{FE})/\chi_a $
3.50	1.6970	1.6936	0.20
4.00	3.8683	3.8698	0.04
4.50	5.9175	5.9292	0.20
5.00	7.9167	7.9462	0.37
6.00	11.924	12.020	0.80
7.00	16.078	16.292	1.33
8.00	20.454	20.868	2.02

TABLE 1. Accuracy of finite element approximation of bifurcation points

The value of R_∞ was chosen by looking at the convergence of the electrical pressure $\Delta\Pi_E$ on given interfaces for increasing values of R_∞ and with regular meshes. This value was taken as $R_\infty = 8$ for $A < 4$ and $R_\infty = 2A$ for $A > 4$. The algorithm was programmed in FORTRAN and calculations were made on the CONVEX-240 at the University of Seville. A convergence study has shown that, for the situations considered in this paper, $10(\text{axial}) \times 14(\text{radial})$ elements are enough to keep errors within 1%. The geometric progression ratio between element lengths was chosen to be 1.2 for the axial and radial directions. The total number of unknowns ($N+M+2$) was 632 and one Newton iteration took about 2.4 s of CPU time.

The accuracy of these finite-element approximations has been tested by computing the critical values of τ in the absence of electric field with or without gravity, and the critical values of χ for cylindrical shapes, i.e. $\tau = 1$ and $B = 0$. The numerically obtained critical values τ_c for $B = 0$ have errors compared with the analytical results of Martínez (1986) that are less than 0.06%. The numerical critical values χ_c are compared with the analytical values (González *et al.* 1989) in table 1 for the case $\beta = 0.55$. This indicates that the accuracy is governed by the electrical problem.

From the table we see that the accuracy of this finite-element approximation decreases with increasing slenderness \mathcal{A} . As an explanation, figure 4 shows some computed critical eigenvector shapes. These indicate a shifting of the maximum towards the extremes of the bridge for increasing \mathcal{A} , a finer mesh near the contact lines then being necessary to maintain the accuracy. A reduction in the errors was subsequently verified.

4. Results and discussion

Most of the following results will be for the case in which permittivity ratio $\beta = 0.55$, slenderness values $\mathcal{A} < 7$ and the Bond number is of small value in order to compare with known theoretical and experimental data given in González *et al.* (1989) and with the Lyapunov–Schmidt method (González & Castellanos 1993). First, we will compute the bifurcation diagrams for liquid bridges in the absence of gravity then subsequently include the effect of a residual gravity.

4.1. Absence of gravity

Let us recall briefly the main features of the equilibrium shapes before considering the nonlinear bifurcation diagrams. In figure 5 we present a stable liquid bridge and equipotentials of the linear potential perturbation, i.e. $\Psi = \Phi - z$, for two applied electric field strengths in the case $\mathcal{A} = 3$, $\tau = 2$. Ψ is the contribution of the polarization charges to the total potential. Because there is no gravitational force the shapes are reflectionally symmetric and the equipotential is antisymmetric about the midplane $z = 0$. This leads to a symmetric electrical pressure. The main effect of the electric field is to align the interface along its direction. The same behaviour was obtained for different permittivity ratios and volumes (Ramos & Castellanos 1991).

4.1.1. The cylindrical solution

The cylinder exists for any value of β, χ, \mathcal{A} , provided $\tau = 1$ and $B = 0$, and it is given by:

$$f(z) = 1, \quad \Delta\Pi = -1 - \frac{1}{2}(\beta - 1)\chi, \quad \Phi(r, z) = z. \quad (21)$$

It is well known from the studies of Plateau and Rayleigh that in the absence of an electric field, the cylinder is stable for \mathcal{A} values lower than π . At the stability limit there is a subcritical bifurcation with the bifurcation eigenvector showing an antisymmetric shape about the midplane $z = 0$ (Martínez 1983; Vega & Perales 1983). When the electric field is imposed, the bifurcation criterion for slenderness increases as a function of the applied electric field, i.e. $\mathcal{A}_c = \mathcal{A}_c(\chi)$, and the bifurcation eigenvector is also antisymmetric (González *et al.* 1989).

Here we have extended the study of the bifurcating family to finite amplitude perturbations and arbitrary values of the electric field. Shown in figure 6 is the amplitude of the bifurcating family for $\beta = 0.55$ and different \mathcal{A} values in terms of the parameter

$$\epsilon = \left(\frac{1}{2\mathcal{A}} \int_{-\mathcal{A}}^{\mathcal{A}} (f(z) - 1)^2 dz \right)^{\frac{1}{2}}, \quad (22)$$

which is the L_2 norm measure of the distance from the equilibrium shape to the cylindrical one, as a function of χ . From this figure it is evident that the bifurcation remains subcritical, the stable cylinders are those with χ greater than the bifurcating one. Each point on the bifurcating branches represents two possible non-symmetrical

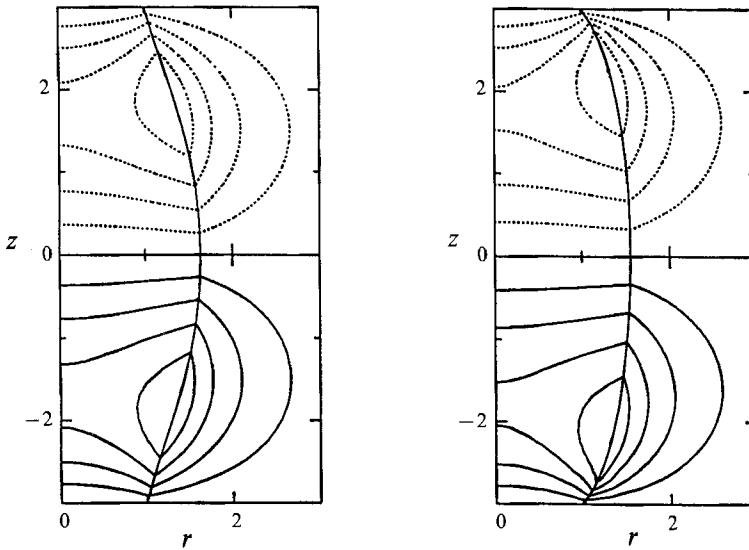


FIGURE 5. Equipotentials of $\Psi = \Phi - z$ for a liquid bridge with $\tau = 2$, $\beta = 0.5$, $A = 3$ subjected to an electric field: (a) $\chi = 0.01$ and (b) $\chi = 5$. Equipotential values grow from dotted lines to solid ones.

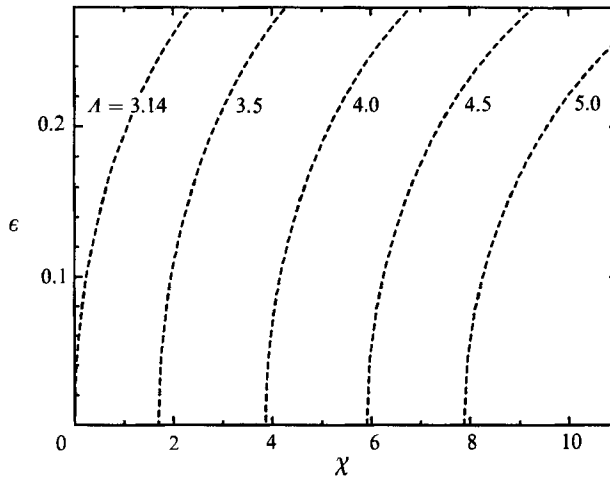


FIGURE 6. The effect of A on liquid bridge stability: ϵ as a function of χ of the bifurcating branches for liquid bridges with $\tau = 1$, $\beta = 0.55$.

shapes, with the neck above or below the midplane $z = 0$. Locally the bifurcating branches are of the form

$$\chi = \chi_c + \frac{1}{2}\kappa\epsilon^2, \tag{23}$$

where κ is the curvature. The computed κ values grow with A . For example, $\kappa = 46.8$ for $A = 3.142$ and $\kappa = 73.6$ for $A = 5$. Hence, the liquid bridge is more sensitive to finite-amplitude perturbations of a given shape as A increases. However, we should bear in mind that to impose a given deformation on the interface may be more demanding energetically when there is an electric field.

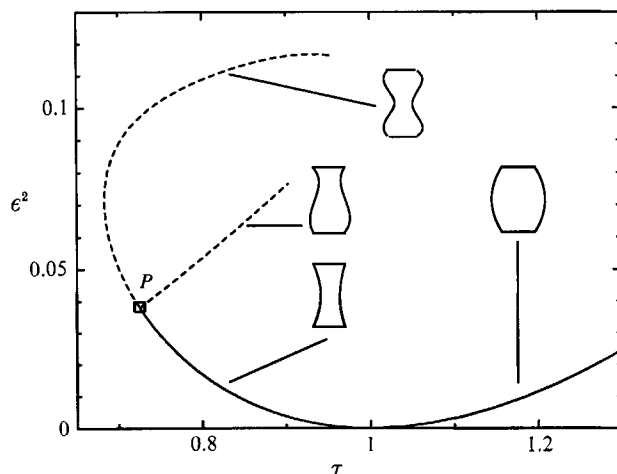


FIGURE 7. ϵ^2 as a function of τ for a liquid bridge with $A = 2.6$, $\chi = 0$. Stable shapes are represented by a solid line.

4.1.2. Arbitrary volume

In the absence of an electric field, static considerations have shown that when the minimum volume stability limit is reached a bifurcation to unstable equilibrium shapes occurs whose character depends on the slenderness (Meseguer, Sanz & Rivas 1983; Sanz & Martínez 1983). For values of $A < 2.128$, the stability criterion is marked by a limit point and consequently the critical eigenvector carries all the symmetry of the equilibrium state. Accordingly the breaking process should be symmetrical leading in the final state to two drops of equal volume. On the contrary for $A > 2.128$ the stability criterion is marked by a bifurcation point with a non-symmetrical bifurcating family. This breaking of symmetry would lead to a rupture of the liquid bridge in two unequal drops. Experiments show a symmetrical ($A < 2.128$) or non-symmetrical ($A > 2.128$) disruption of the liquid bridge corresponding to turning points or simple bifurcation points (Sanz & Martínez 1983), in agreement with the theoretical findings.

Figure 7 shows the finite bifurcation diagram computed by our method for a liquid bridge of $A = 2.6$ in the absence of an electric field. The order parameter is ϵ^2 , the squared distance from the cylindrical shape. Only those liquid bridges with non-dimensional volumes greater than $\tau_c = 0.725$, the bifurcation volume, are stable. We may form, for example, a cylindrical liquid bridge. If we now extract liquid in a quasi-static way we move leftwards along the equilibrium curve until we get to the point P , corresponding to $\tau_c = 0.725$, where a non-symmetrical bifurcating family exists, leading to a non-symmetrical disruption of the newly formed liquid bridge.

Similar bifurcation diagrams are obtained for increasing values of A , the main effect being a rightwards displacement of the point P along the corresponding curve, i.e. for $A = \pi$ it is placed at $\tau = 1$. For decreasing values of A the bifurcating branch is displaced leftwards along the corresponding curve. For $A = 2.128$ the point P reaches the turning point. Further decreasing A moves P along the upper branch of the symmetric shape family. Thus for $A < 2.128$ the bifurcating branch location does not define the stability criterion anymore.

The role of the parameter A upon the nature of the disruption of the liquid bridge has been considered in some detail because the influence of the electric field upon the stability resembles in many ways the role played by A^{-1} . This will be illustrated in

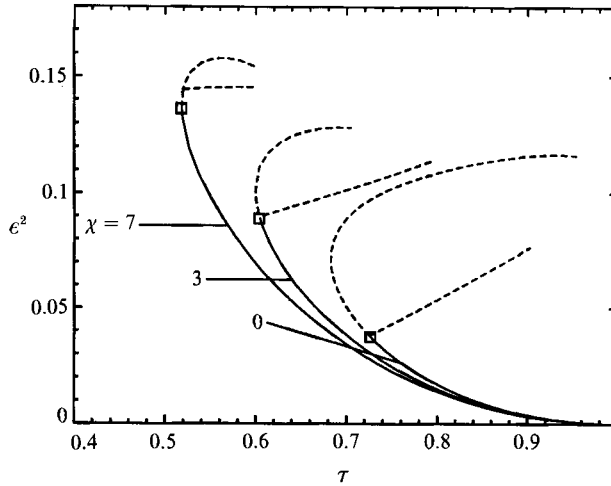


FIGURE 8. The effect of χ on the stability: ϵ^2 as a function of τ for a liquid bridge with $A = 2.6$, $\beta = 0.55$.

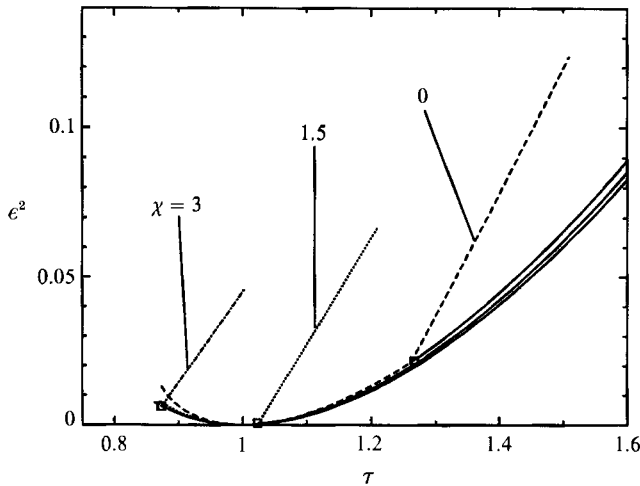


FIGURE 9. The effect of χ on the stability: ϵ^2 as a function of τ for a liquid bridge with $A = 3.5$, $\beta = 0.55$.

figures 8 and 9. In figure 8 the influence of the electric field upon the stability of a liquid bridge of $A = 2.6$ is depicted. We see that the electric field modifies the bifurcation diagram in two ways. First, the position of the turning and bifurcation points changes towards smaller values of τ : a consequence of the stabilizing effect of the electric field. Secondly, the relative location of the two critical points is shifted occasionally giving rise to an interchange of the turning and bifurcation points, similar to the case of A decreasing. Thus, for a cylindrical liquid bridge subjected to an electric field, $\chi = 7$, extracting fluid will allow us to attain a minimum critical volume $\tau_c = 0.518$ that will then break into two equal drops.

Figure 9 illustrates the stabilizing effect of the electric field for a liquid bridge of $A = 3.5$. On increasing the electric field the bifurcating branch is displaced leftwards thus decreasing the critical volume physically attainable. We could continue to increase the value of χ and again we would have an interchange of the turning and

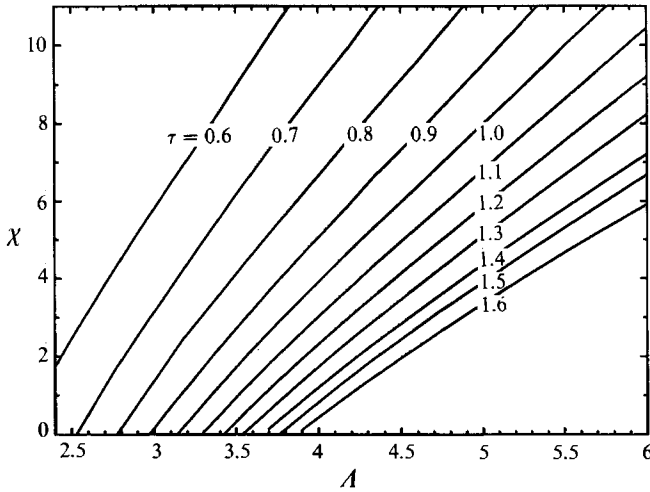


FIGURE 10. Neutral stability curves in the (A, χ) -plane for different τ . The permittivity ratio is fixed, $\beta = 0.55$.

bifurcation point, as illustrated in figure 8. As in this case $A > \pi$, the cylinder is unstable in the absence of electric field and the bifurcation for $\chi = 0$ occurs for $\tau > 1$. The effect of an increase in A is to shift the critical points to greater values of τ .

Figure 10 shows the neutrally stable, singular points in the (A, χ) -plane for a set of values of τ and fixed $\beta = 0.55$. A liquid bridge can be held stable only if the set (χ, A) belongs to the upper region delimited by the corresponding τ curve. For $\chi = 0$, the results of minimum volume without electric field are recovered. The curve $\tau = 1$ corresponds to the bifurcation curve of the cylindrical family. We see that the increment of the electric field allows us to elongate liquid columns of a given τ . Also, we can reduce the volume of a bridge, keeping it stable, by increasing the electric field.

Finally, we examine briefly the role of the parameter β . Because the statics of the liquid bridge is dominated by the interfacial dielectric force, and this force is zero for $\beta = 1$ (equal permittivities of the outer and inner liquids) it is clear that β has to be different from 1. It has been shown (González *et al.* 1989) that β and β^{-1} play a similar role, it being of little consequence which of the two liquids forms the bridge. In fact the difference between β and β^{-1} may be ascribed to the presence of a finite curvature of the interface and should be zero for a plane interface. In figure 11 the minimum critical volume for a liquid bridge of fixed slenderness $A = 3$ as a function of χ is represented. We see that for $\beta = 1$ the critical volume is independent of the electric field, $\tau_c = 0.914$, whilst for values of β differing from unity the critical volume decreases. For a given value of χ the latter volume decreases as the permittivity difference between the outer and inner liquid increases. Notice that for $\beta = 3$ and for $\beta = 0.3 \approx \frac{1}{3}$ the two curves are close to each other, agreeing with the qualitative symmetry of the system to the interchange of the liquids.

4.2. Gravity effect

The influence of an axial gravity on the stability of liquid bridges is well known (Vega & Perales 1983; Meseguer *et al.* 1990). The axial gravitational forces distinguish between a non-symmetrical shape and its reflected one around the midplane $z = 0$. This breaking of symmetry excludes the cylinder as a possible solution for the case

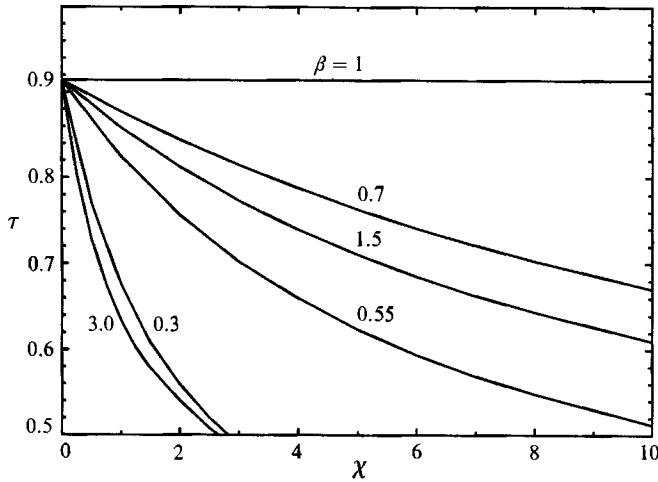


FIGURE 11. Neutral stability curves in the (χ, τ) -plane for different β . The slenderness is fixed, $A = 3$.

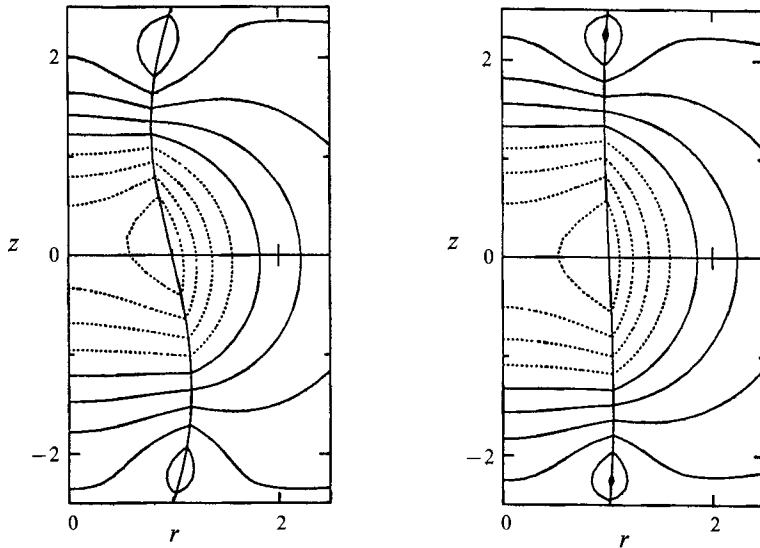


FIGURE 12. Equipotentials of $\Psi = \Phi - z$ for a liquid bridge with $\tau = 1$, $\beta = 0.5$, $A = 2.5$ subjected to an electric field and an axial gravity $B = 0.06$. (a) $\chi = 0.01$ and (b) $\chi = 5$. Equipotential values grow from dotted lines to solid ones.

$\tau = 1$. Instead equilibrium forms will be amphoric, with the amphora neck above (below) the midplane for positive (negative) values of the Bond number. Also, an axial gravity causes the liquid bridge to be less stable for a fixed slenderness or, alternatively, the critical slenderness decreases as we increase the gravitational Bond number for a given τ . Here we extend this analysis to determine the effect of electric fields on the equilibrium shapes and stability. As already mentioned we will restrict the analysis to values of the Bond number $B < 0.1$.

As in the absence of gravity we present first the equilibrium shapes of liquid bridges subjected to an applied electric field in the presence of gravity. In figure 12 liquid shapes and equipotentials of $\Psi = \Phi - z$ are shown for a liquid bridge subjected

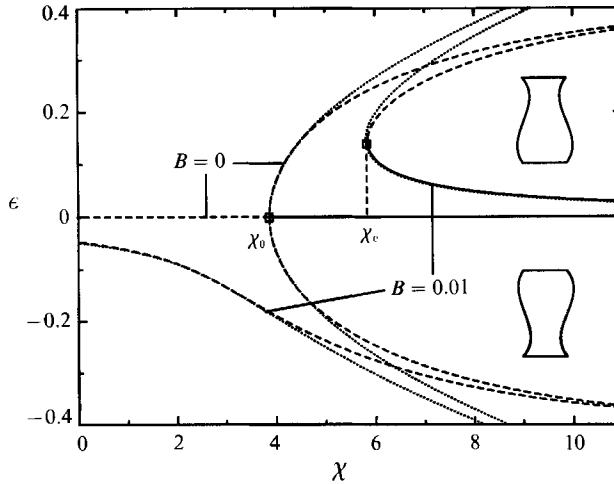


FIGURE 13. The effect of B on liquid bridge stability: ϵ as a function of χ for liquid bridges with $\tau = 1$, $A = 4$, $\beta = 0.55$. \cdots , curves obtained by the Lyapunov-Schmidt method for comparison.

to a gravity strength $B = 0.06$ for two different values of χ in the case $\tau = 1$, $A = 2.5$. These shapes correspond to stable liquid bridges. The alignment of the interface with the symmetry axis for increasing field is evident. We see that for $B \neq 0$ these shapes are no longer reflectionally symmetric but they resemble the non-symmetric bifurcating family of the case $B = 0$, which is the reason of the breakdown of the pitchfork bifurcation. The potential perturbation, Ψ , is close to being symmetric and so the electrical pressure perturbation is close to being antisymmetric. In this sense the electrical pressure perturbation follows the symmetry of the shapes.

4.2.1. Quasicylinders ($\tau = 1$)

The influence of axial residual gravity on the stability of cylindrical liquid bridges has been analysed in detail in Vega & Perales (1983). It has been shown that the effect of gravity is to change the nature of the bifurcation from a pitchfork bifurcation to two separated branches with the stable branch now losing its stability through a limit point. A semianalytical study based on the Lyapunov-Schmidt method has also included the effect of the electric field (González & Castellanos 1993). From the latter local study we see that gravity always breaks the subcritical pitchfork bifurcation in two isolated solutions. Here we extend the previous analysis to finite-amplitude perturbations of the equilibrium shape.

Figure 13 shows the deformation ϵ as a function of χ for $\tau = 1$ and $A = 4$ in two cases: without gravity, $B = 0$, and with a residual gravity, $B = 0.01$. For comparison, the local diagram obtained by the Lyapunov-Schmidt method (González & Castellanos 1993) is also presented (dotted line). Negative values of ϵ correspond to shapes that have their neck below the plane $z = 0$. As the gravitational field has broken the original symmetry, the subcritical bifurcation disappears giving two separate equilibrium families. The stable branch is the one connected to the stable cylinders when $\chi \rightarrow \infty$ and $\epsilon \rightarrow 0$. As is evident from the figure, the new critical electric field is determined by a limit point and is greater than the non-gravitational bifurcation field. From the comparison with the local method we see that there is a very good agreement for $|\epsilon| < 0.2$. This can be used as a rule to estimate the range of validity of the local results. For this Bond number, $B = 0.01$, the computed critical

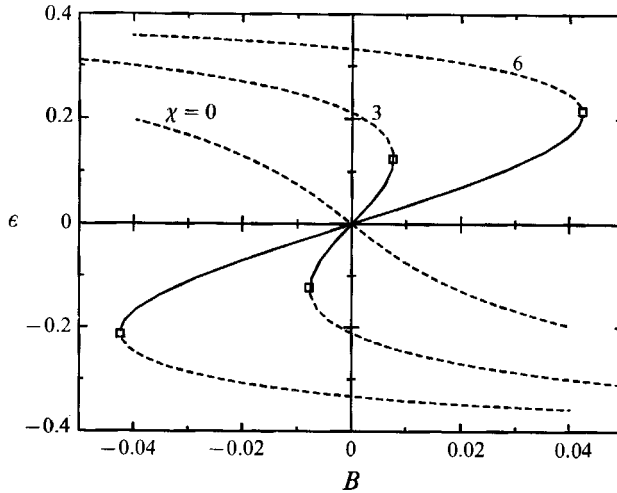


FIGURE 14. The effect of χ on liquid bridge stability: ϵ as a function of B for liquid bridges with $\tau = 1$, $A = 4$, $\beta = 0.55$.

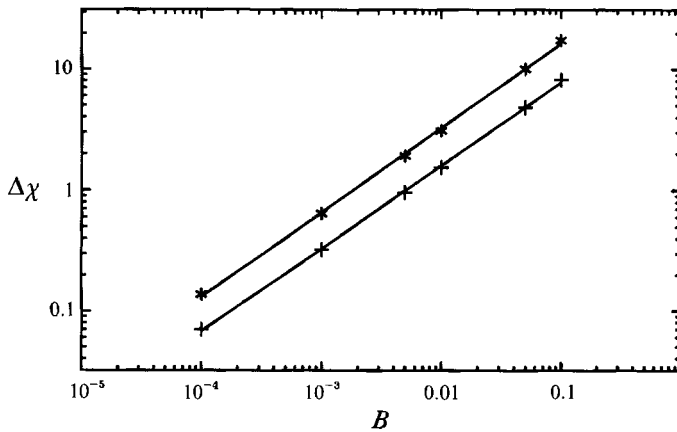


FIGURE 15. Critical electrical number shift $|\chi_c - \chi_0|$ as a function of B for two different A : +, $A = 3.5$; *, $A = 5$. The permittivity ratio is $\beta = 0.55$.

values of χ are $\chi_c = 5.856$ by the present method and $\chi_c = 5.814$ by the perturbation method, a difference only of 0.7%.

Figure 14 shows the deformation ϵ as a function of B for three values of χ in the case $\tau = 1$, $A = 4$. Negative values of ϵ correspond to inverted amphoras. It is obvious from the figure that there exists a complete symmetry between the cases $B > 0$ and $B < 0$. The number of solutions passes from one to three owing to the electric field. For $\chi = 0$ the equilibrium shapes are not stable (notice that $A = 4 > \pi$), the reason for the appearance of the stable shape region (between the two limit points) is the stabilizing effect of the electric field. This region grows with the electric field.

The shift in critical value of the electrical parameter as a function of B is depicted in figure 15 on a logarithmic scale. The theory of bifurcation predicts a change of the critical χ with respect to the no-gravity bifurcation χ proportional to $B^{\frac{2}{3}}$, i.e. $|\chi_c - \chi_0| = cB^{\frac{2}{3}}$, for small B , based only in symmetry arguments (González & Castellanos 1993). Two cases with different A are presented. The tangent of these

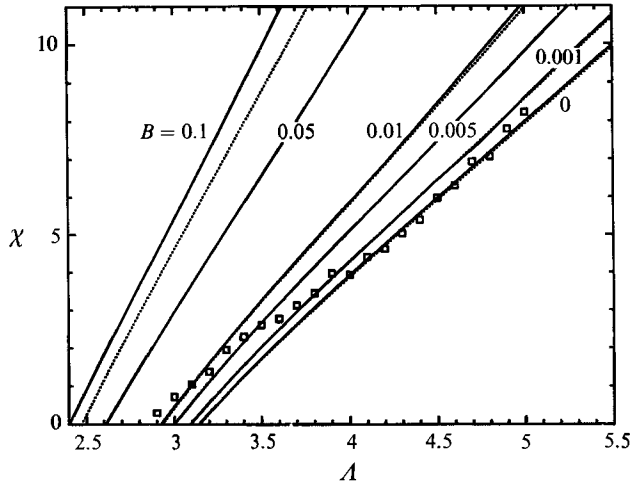


FIGURE 16. Neutral stability curves in the (A, χ) -plane for different B in the case $\beta = 0.55$, $\tau = 1$, the Lyapunov-Schmidt method. \square , experimental data.

curves numerically obtained approaches 0.66. Also we see that the proportionality constant c increases for increasing A indicating a greater sensitivity of the liquid bridge with B .

Figure 16 shows the neutral stability curves in the (A, χ) -plane for bridges with cylindrical volume, i.e. $\tau = 1$, and for different values of B . For comparison, the neutral stability curves (dotted lines for $B = 0, 0.001, 0.01, 0.1$) obtained by the Lyapunov-Schmidt method are presented. The experimental data given by González *et al.* (1989) are also shown. As in figure 10 the stable region is above each curve. We can see that the curve corresponding to $B = 0$ is the maximum limit of stability and the gravity effect is to increase the necessary field to hold the bridge. The neutral stability curves diverge for increasing A showing that the gravity influence is more important as the slenderness increases. As in the absence of the electric field the liquid bridge is more sensitive to B with A . From a comparison with the local method we see a fair agreement for values of $B \leq 0.01$ so the transition from $B = 0.01$ to $B = 0.1$ marks an accuracy limit of the local results in the chosen range of A . The comparison with the experimental data tells us that, for low values of the electric field, the experimental points lie on the curve corresponding to $B = 0.01$ and these points approach $B = 0$ for large values. Since the temperature in those experiments was not carefully controlled the experimental points could correspond to different values of the Bond number, as the density difference is dependent on temperature. Nevertheless, this discrepancy may be due to the nature of the anchoring (an increment of the local field close to the rings) and, in any case, a more careful determination of the physical parameters seems to be necessary to have a better agreement.

4.2.2. Arbitrary volume

Let us now consider liquid bridges with $\tau \neq 1$. For these cases the influence of B on the equilibrium shape, as well as the determination of the critical volume in the absence of the electric field, has been obtained numerically. The results show a greater sensitivity of the liquid column to the number B for increasing values of the slenderness (Meseguer & Sanz 1985; Meseguer *et al.* 1990).

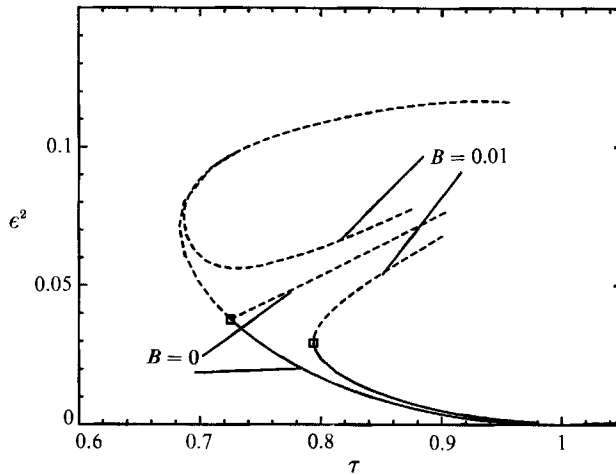


FIGURE 17. The effect of B on liquid bridge stability: ϵ^2 as a function of τ for the case $A = 2.6$ and $\chi = 0$.

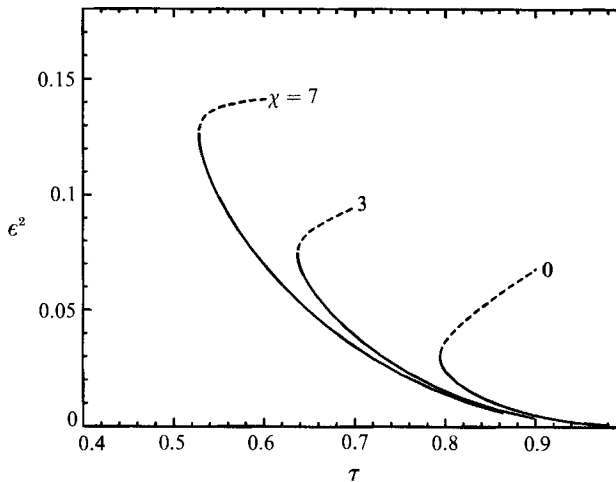


FIGURE 18. The effect of χ on liquid bridge stability: ϵ^2 as a function of τ for the case $A = 2.6$ and $B = 0.01$.

We present in figure 17 the bifurcation diagram computed using our method for the case $A = 2.6$ for $B = 0$ and $B = 0.01$. It is apparent from the figure that the bifurcation point has disappeared and the symmetric and non-symmetric family branches have given rise to two separated branch solutions. The stable branch loses its stability through a limit point but contrary to the case where gravity is absent the disruption is now non-symmetrical. The new critical value of the volume is greater showing the destabilizing nature of the gravitational forces.

The presence of the electric field modifies this diagram in three ways (see figure 18). First, for a given value of the Bond number and a fixed value of τ the electric field decreases the value of ϵ . This means that the shape becomes more cylindrical a fact already familiar to us. Secondly, the stable branch (the only one shown to avoid unnecessary details) increases in length with the electric field, stabilizing the column for smaller values of the liquid volume. Thirdly, the relative change of the critical τ

with respect to the non-gravitational bifurcation τ (see figure 8), i.e. $\Delta\tau = |\tau_c - \tau_0|$, is smaller for increasing values of χ . In the present case, $\Delta\tau$ decreases from $\Delta\tau = 0.07$ for $\chi = 0$ to $\Delta\tau = 0.01$ for $\chi = 7$. The same happens for decreasing A , so as a general result liquid bridges are less sensitive to a residual axial gravity when either χ increases or A decreases.

5. Conclusions

An algorithm based upon the Galerkin/finite element method has been applied to determine equilibrium shapes and stability limits of axisymmetric liquid bridges anchored between two plane parallel plates subjected to a potential difference and in the presence of gravity.

The effect of the applied electric field on the bridge shapes is to make them *more cylindrical*, i.e. to align the interface with its vertical axis. This qualitative behaviour is independent of which liquid forms the bridge, of its volume and of the residual gravity. This is the reason why the electric field always increases the stability of the liquid column.

Axisymmetric liquid bridges may lose their stability either in limit or in bifurcation points for the case $B = 0$ and in limit points for the case $B \neq 0$. For $B = 0$, the limit points will be the stability limit if τ is small enough. Since the electric field allows us to reduce the volume necessary to hold a liquid bridge, it can change the way of the breaking process towards a symmetrical disruption because limit and bifurcation points approach each other for decreasing τ . In the absence of the electric field a similar effect happened for decreasing A .

The liquid columns of the bifurcating family have non-symmetric shapes that resemble the shapes found in the presence of gravity. Gravity breaks the original symmetry and distinguishes between the two bifurcating shapes, with its neck above or below the plane $z = 0$, this being the reason for the breaking in the bifurcation diagram. Thus the effect of residual axial gravity upon the stability is very pronounced. This effect decreases with A^{-1} , showing that the sensitivity to gravity increases with the slenderness. Similarly, for a fixed A the gravity effect decreases as χ increases. We may then conclude that the effect of the electric field on liquid bridges is somewhat similar to the effect of the inverse of the slenderness.

REFERENCES

- BASARAN, O. A. & SCRIVEN, L. E. 1989 Axisymmetric shapes and stability of charged drops in an external electric field. *Phys. Fluids A* **1**, 799–809.
- BEZDENEJNYKH, N. A., MESEGUER, J. & PERALES, J. M. 1992 Experimental analysis of stability limits of capillary liquid bridges. *Phys. Fluids A* **4**, 677–680.
- GONZÁLEZ, H. & CASTELLANOS, A. 1993 The effect of residual gravity on the stability of liquid columns subjected to electric fields. *J. Fluid Mech.* **249**, 185–206.
- GONZÁLEZ, H., MCCLUSKEY, F. M. J., CASTELLANOS, A. & BARRERO, A. 1989 Stabilization of dielectric liquid bridges by electric fields in the absence of gravity. *J. Fluid Mech.* **206**, 545–561.
- IOOSS, G. & JOSEPH, D. D. 1980 *Elementary Stability and Bifurcation Theory*. Springer.
- JACKSON, J. D. 1975 *Classical Electrodynamics*. Wiley.
- KELLER, H. B. 1977 Numerical solution of bifurcation and nonlinear eigenvalue problems. In *Applications of Bifurcation Theory* (ed. P. H. Rabinowitz). Academic.
- MARTÍNEZ, I. 1983 Stability of axisymmetric liquid bridges. In *Materials Sciences under Microgravity* ESA SP-191, pp. 267–273.
- MARTÍNEZ, I. 1986 Liquid bridge stability data. *J. Cryst. Growth* **78**, 369–378.

- MESEGUER, J. & SANZ, A. 1985 Numerical and experimental study of the dynamics of axisymmetric slender liquid bridges. *J. Fluid Mech.* **153**, 83–101.
- MESEGUER, J., SANZ, A. & RIVAS, D. 1983 The breaking of axisymmetric noncylindrical liquid bridges. In *Materials Sciences under Microgravity* ESA SP-191, pp. 261–265.
- MESEGUER, J., SANZ, A. & PERALES, J. M. 1990 Axisymmetric long liquid bridges stability and resonances. *Appl. Microgravity Tech.* **4**, 186–192.
- RAMOS, A. & CASTELLANOS, A. 1991 Shapes and stability of liquid bridges subjected to a.c. electric fields. *J. Electrostatics* **26**, 143–156.
- SAITO, H. & SCRIVEN, L. E. 1981 Study of coating flow by the finite element method. *J. Comput. Phys.* **42**, 53.
- SANZ, A. & MARTÍNEZ, I. 1983 Minimum volume for a liquid bridge between equal disks. *J. Colloid Interface Sci.* **93**, 235–240.
- STRANG, G. & FIX, G. 1973 *An Analysis of the Finite Element Method*. Prentice-Hall.
- VEGA, J. M. & PERALES, J. M. 1983 Almost cylindrical isorotating liquid bridges for small Bond numbers. In *Materials Sciences under Microgravity* ESA SP-191, pp. 247–252.